PHILOSOPHICAL TRANSACTIONS OF THE ROYAL SOCIETY A MATHEMATICAL, PHYSICAL & ENGINEERING SCIENCES

The Structure of the Chromosphere-Corona Transition Region from Limb and Disk Intensities

W. M. Burton, Carole Jordan, A. Ridgeley and R. Wilson

Phil. Trans. R. Soc. Lond. A 1971 **270**, 81-98
doi: 10.1098/rsta.1971.0063

Phil. Trans. Roy. Soc. Lond. A. **270**, 81–98 (1971) [81]
Printed in Great Britain

The structure of the chromosphere–corona transition region from limb and disk intensities

By W. M. Burton, Carole Jordan, A. Ridgeley and R. Wilson
Astrophysics Research Unit, Culham Laboratory, Abingdon, Berkshire

During a rocket flight in April 1969, spectra were obtained of a region of the solar disk and at the solar limb. The absolute disk intensities derived from these data have been used to compute models of the transition region, making the assumptions that the relative abundances of different elements remain constant throughout the atmosphere, and that the electron pressure varies according to the equation of hydrostatic equilibrium. The models obtained are characterized by very steep temperature gradients. The relative intensities of emission lines in the disk and limb spectra have enabled the height of the emitting regions to be determined independently of the above assumptions, and independently of atomic data and absolute intensities. A comparison is made of the structure found by the two methods, and within the accuracy of the present data these are consistent. Emission from low temperature ($\sim 10^4$ K) material is observed from heights up to 10^4 km above the transition region, and this probably originates in spicules.

1. Introduction

Analyses of the emission spectrum from the whole Sun in the extreme u.v. have led to models of the chromosphere-corona transition region which are characterized by steep temperature gradients (Pottasch 1964; Jordan 1965; Athay 1966). In order to derive these models it was necessary to assume that either the electron densities or electron pressure are known and that the abundances of the elements remain constant throughout the atmosphere. Delache (1967) has questioned the validity of these interpretations, pointing out that thermal diffusion can change the abundances of elements relative to that of hydrogen. If these changes existed and were ignored, the temperature gradients derived from total line intensities would be over-estimated.

An alternative method of deriving the temperature gradient is to observe the relative intensities of lines measured at the centre of the solar disk and at the solar limb (Burton, Ridgeley & Wilson 1967). This limb/disk ratio method has the advantages that the temperature gradient derived does not depend on absolute photometry or on atomic data such as collisional excitation rates; nor does it depend on the assumption of constant element abundances. However, there are disadvantages in that many of the strong lines are optically thick on the limb and the effects of inhomogeneities such as spicules may be important. These problems can be overcome by using lines which are certainly optically thin, such as intercombination lines.

The spectroscopic instrumentation which has been developed for use with the sun-stabilized Skylark rocket vehicle has been described in the paper by Burton *et al.* (1967). Improved instrumentation was carried in the payload of a sun-stabilized Skylark rocket, SL 606, which was flown from Woomera, South Australia, on 17 April 1969. The present paper describes the new instrumentation used on that flight, the analysis of absolute disk intensities and the method of analysis of the relative limb and disk intensities. A complete wavelength list of lines observed and their identifications will be published separately (Burton & Ridgeley 1970).

2. Instrumentation

The basic optical system was similar to that used for earlier flights (Burton *et al.* 1967), except that an off-axis parabolic mirror was used to image the Sun at the spectrometer slit with good spatial resolution. The mirror was made of fused silica and was uncoated, which gave the advantages that (i) scattered light from the mirror was kept to a minimum, and (ii) good discrimination against visible light was obtained at shorter wavelengths. The spectrograph used a 1200 line/mm grating, blazed at 100 nm, and the wavelength region covered was 50 to 250 nm in the first order. The replica grating was mounted on a red glass blank and was coated with a thin layer of zinc sulphide in order to give further discrimination against visible light. The use of the 'outside order' spectrum gave a reduced astigmatism at short wavelengths and thus provided some compensation for the lower efficiency below 100 nm. The orientation of the collector mirror was controlled by a servo system whose capability was extended over the earlier version (Black & Shenton 1966), to allow programming during flight. Three exposures were taken with the slit set first outside the south polar limb, chosen to avoid active regions, and two exposures were then taken on the disk at a point 5′ inside the limb. The spectra were recorded on Eastman–Kodak 101–01 emulsion.

3. Data

The limb and disk spectra obtained contained a sufficient number of optically thin lines for the structure to be derived from these lines alone. However, the photometric quality of the data was impaired by the deterioration suffered by the films during the week's delay in locating the payload after the parachute failed to deploy.

The optical system was precalibrated in the manner described by Burton, Ridgeley & Hatter (1968). For the limb/disk ratios the absolute film sensitivity and overall instrumental efficiency need not be known, only the response curve of the film. For absolute intensities all the above factors are necessary. The internal scatter in results from the three limb and two disk exposures suggests that the ratios and absolute intensities are accurate to within about a factor of two.

The method of analysis described in § 5 and appendix I depends on knowing the slit function $f(x)$ which is the form of the image as seen by the slit. This function was determined from pre-flight laboratory measurements of a stationary image which were then convoluted with the flight pointing noise derived from the telemetry records, and the projected slit width of 8″. The position of the slit was set before launch but was not measured in flight. The heights derived are therefore relative positions of regions emitting the different lines. Ideally the position of the slit would be derived from limb/disk ratios in the continuum, making use of known limb darkening coefficients.

Table 1 lists the wavelengths of the lines for which it was possible to derive both limb and disk intensities, the element and stage of ionization producing the line, the observed limb flux and the disk flux expressed as the equivalent emission from the whole disk. The identifications have been made using Moore (1950, 1965), Kelly (1968), Junkes, Salpeter & Milazzo (1965) and Burton *et al.* (1967). The source of each identification is indicated in table 1. The disk observations were made 5′ inside the polar limb and were corrected to refer to the centre of the disk before the limb/disk ratios were derived. The correction has been applied to all lines except permitted lines of neutral atoms, which have optical depth greater than unity over the whole disk.

TABLE 1. INTENSITY DATA FROM SL 606

λ/nm	ion	multiplet	I (limb) / 10^{-4} μJ m^{-2} s^{-1}	I (total disk) / μJ m^{-2} s^{-1}	I (limb) / I (disk)
94.97	H I	4	6.6	2.8	0.087
97.70	C III	1	62	23	0.098
98.98	N III	1	10	1.5	0.24
99.16	N III	1	34	1.8	0.72
102.57	H I	2	39	13	0.11
103.19	O VI	1	67	49	0.50
103.63	C II	2	7.7	1.2	0.24
103.70	C II	2	11	1.6	0.25
103.76	O VI	1	48	2.8	0.62
108.50	He II	14	14	1.0	0.51
108.57	N II	1	13	1.5	0.32
117.57	C III	4	48	8.0	0.22
119.04	Si II	u.v. 5	8.5	1.1	0.30
120.65	Si III	u.v. 2	50	13	0.14
121.83	O V	B	25	1.1	0.86
123.88	N V	1	41	1.6	0.97
124.28	N V	1	29	1.1	0.99
125.38	S II	1	6.4	0.6	0.36
125.65	C I, Si I	K, K	3.1	9.0	0.13
125.95	S II	1	7.4	0.6	0.40
126.04	Si II	u.v. 4	6.3	0.8	0.28
126.47	Si II	u.v. 4	25	2.3	0.40
126.64	C I	58	6.2	0.9	0.26
127.48	C I	55, 56	3.3	0.9	0.14
130.10	Si III	u.v. 4	6.2	0.8	0.27
130.22	O I	2	34	7.3	0.17
130.49	O I	2	31	9.6	0.12
130.60	O I	2	29	7.7	0.14
130.93	Si II	3	6.9	1.5	0.17
132.35	S I	8	4.5	0.9	0.18
133.45	C II	1	72	11	0.23
133.57	C II	1	74	19	0.14
135.85	O I	1	17	0.6	0.75
136.41	C I	39	2.7	1.1	0.092
139.38	Si IV	u.v. 1	104	13	0.29
140.11	O IV	B	80	2.3	1.30
140.28	Si IV	u.v. 1	93	5.3	0.65
142.51	S I	5	6.6	3.2	0.078
143.33	S I	5	3.6	2.5	0.054
145.50	Ni II	7	5.3	1.5	0.13
146.33	C I	37	3.6	2.5	0.053
146.74	C I	36	9.9	2.6	0.14
147.30	S I	4	18	1.8	0.39
147.40	S I	3	9.8	3.4	0.11
148.18	C I, S I	34, 4	20	4.6	0.16
148.30	S I	3	12	3.7	0.12
148.66	N IV	B	50	1.3	1.42
151.09	Ni II, C I	6, K	14	1.7	0.29
152.67	Si II	u.v. 2	52	8.5	0.23
153.34	Si II	u.v. 2	60	7.8	0.28
154.52	C I	K	32	14	0.087
154.82	C IV	1	200	33	0.23
155.08	C IV	1	171	16	0.38
155.91	Fe II	45	93	6.4	0.53
156.14	C I	3	81	16	0.19
156.38	Fe II	45	81	5.4	0.55
156.68	Fe II	44	57	3.6	0.57
156.80	Fe II	45	42	1.9	0.81

PHILOSOPHICAL TRANSACTIONS OF THE ROYAL SOCIETY A MATHEMATICAL, PHYSICAL & ENGINEERING SCIENCES

TABLE 1. (*cont.*)

λ/nm	ion	multiplet	I (limb) / 10^{-4} μJ m^{-2} s^{-1}	I (total disk) / μJ m^{-2} s^{-1}	I (limb) / I (disk)
157.02	Fe II	45	81	4.2	0.71
157.13	Si I	K	24	1.3	0.66
157.38	Fe II, Si I	45, 40	75	5.0	0.55
157.49	Fe II	45	87	7.5	0.43
158.49	Fe II	44	48	3.5	0.50
158.83	Fe II	44	57	5.7	0.37
159.23	Si I	36	15	1.7	0.32
159.79	Si I	34, 35	18	1.7	0.39
160.26	Fe II	V	33	1.9	0.64
160.84	Fe II, C I	8, K	31	3.4	0.33
161.09	Fe II	43	71	3.1	0.86
161.28	Fe II	43	71	4.0	0.66
161.85	Fe II	8	21	2.2	0.36
162.17	Fe II	8	26	1.2	0.78
162.31	Fe II	43	46	2.5	0.69
162.55	Fe II	43	88	3.5	0.94
163.27	Fe II	43	47	3.4	0.51
163.39	Fe II	43	76	3.4	0.82
163.74	Fe II	42	81	4.7	0.64
164.05	He II	12	250	9.2	0.98
164.36	Fe II	42	59	3.9	0.56
164.94	Fe II	42	45	2.5	0.67
165.45	Fe II	42	80	2.4	1.20
165.70	C I	2	80	41	0.071
165.95	Fe II	40	130	8.0	0.59
166.32	Fe II	40	74	3.1	0.89
167.08	Fe II, Al II	40, 2	120	23	0.20
167.35	Fe II	102	46	1.9	0.90
167.43	Fe II	41	85	3.1	1.0
167.94	Fe II	102	46	2.4	0.69
168.10	Fe	V	62	3.4	0.69
168.65	Fe II	40	170	8.8	0.74
169.68	Fe II	38	88	13	0.26
170.20	Fe II	38	150	10	0.53
171.30	Fe II	38	170	12	0.49
172.48	Fe II	39	160	4.2	1.40
172.64	Fe II	38	140	8.2	0.65
180.80	Si II	u.v. 1	380	> 150	< 0.095
181.69	Si II	u.v. 1	300	> 260	< 0.038
181.74	Si II	u.v. 1		> 29	
189.20	Si III	u.v. 1	620	< 55	> 0.42
190.87	C III	B	370	< 60	> 0.23

Notes to Table 1. Where the multiplet number is given the source is Moore (1950); use of a u.v. multiplet number indicates the source is Moore (1965); K indicates Kelly (1968); V indicates Junkes *et al.* (1965); B indicates Burton *et al.* (1967). The usual units of erg cm^{-2} s^{-1} have been converted to μJ m^{-2} s^{-1} (1 erg cm^{-2} s^{-1} = 10^3 μJ m^{-2} s^{-1}).

4. THE STRUCTURE DERIVED FROM ABSOLUTE INTENSITIES

(*a*) *Relative abundances and the mean distribution of* $\int N_e^2 \mathrm{d}h$ *with temperature*

The method of analysis for the absolute intensities of solar u.v. resonance lines has been established by Pottasch (1963). The observed flux from a given line, at the distance of the Earth, is

$$E_{12} = 3.0 \times 10^{-23} f_{12} \int_0^\infty \bar{g} T_e^{-\frac{1}{2}} \frac{N(E)}{N(H)} \frac{N(i)}{N(E)} \frac{N_1}{N(i)} N_e N_H \, e^{-W_{12}/kT_e} \mathrm{d}h \, \mu\mathrm{J\,m^{-2}\,s^{-1}}, \qquad (1)$$

where f_{12} is the oscillator strength; $\bar{g}$ is the integrated Gaunt factor; $N(E)/N(H)$ is the abundance

of the element relative to that of hydrogen; $N(i)/N(E)$ is the ionization equilibrium; $N_1/N(i)$ is the fraction of the ion in the lower level of the transition; for C III, N IV and O V the calculations of Jordan (1970) have been used. For lower ions and Si III the Boltzmann distribution has been used for the metastable populations, and hence $N_1/N(i)$ derived. N_e, N_H are the electron and hydrogen number densities respectively.

Taking $N_1/N(i)$ and 1; $N(E)/N(H)$ as constant over the region where the line is formed; $N_H = 0.80\,N_e$ for $T_e \geqslant 2\times10^4$ K and $\bar{g}$ as constant over the region where the line is formed, equation (1) becomes

$$E_{12} = 2.4\times10^{-23} f_{12}\bar{g}\,\frac{N_1}{N(i)}\,\frac{N(E)}{N(H)}\int_0^\infty N_e^2 g(T)\,dh, \tag{2}$$

where

$$g(T) = T_e^{-\frac{1}{2}}\,\frac{N(i)}{N(E)}\,10^{-5040W_{12}/T_e}. \tag{3}$$

Following Pottasch (1964), the function $g(T)$ has a maximum value $g_m(T)$ at some temperature T_m. Since this function has a fairly sharp maximum, $g(T)$ is removed from the integral and is replaced by $0.70g_m(T)$, i.e. it is assumed that all the emission comes from a region, R, where T_e is within a certain $\pm\Delta T$ of T_m; the factor of 0.70 is the normalization factor. The emission can then be written as

$$E_{12} = 1.7\times10^{-23} f_{12}\bar{g}\,g_m(T)\,\frac{N_1}{N(i)}\,\frac{N(E)}{N(H)}\int_R N_e^2\,dh. \tag{4}$$

The average value used by Pottasch gives reasonably accurate results but in the present analysis the normalization factor for a fixed range of $\lg\Delta T = \pm0.15$ dex and the percentage of the total emission formed in this temperature range has been computed for each line.

Thus for each line,

$$\frac{N(E)}{N(H)}\int_R N_e^2\,dh$$

can be computed. If a sufficient number of lines from different stages of ionization in each element is observed, the relative abundances and the mean distribution of

$$\int_R N_e^2\,dh$$

with temperature can be found. Figure 1 shows the mean curve of

$$\frac{N(C)}{N(H)}\int_R N_e^2\,dh.$$

The atomic data used in the analysis are given in table 2: the temperatures for the singly charged ions are those for the peak value of $N(i)/N(E)$, *not* those for the maximum value of $g(T)$. Since the function $\int N_e^2\,dh$ falls quite rapidly between 10^4 and 3×10^4 K, the density weighting (unknown) should also be included as well as the temperature weighting. If T_m is used, it is found, by iteration, that the region at lower temperatures would give far more emission than is observed. The collisional de-excitation rate is small compared with spontaneous radiative decay for the relevant transitions, and all the photons created where $\tau \lesssim 10^3$ should escape from the atmosphere. The sources of atomic data are as follows: f values from Wiese, Smith & Glennon (1966); $\bar{g}$ from the impact parameter method and tables of Burgess (1964); $g(T)$ and T_m are from the ionization equilibrium calculations of Jordan (1969*a*). The abundances derived are given in table 3, and are all within a factor of two of those tabulated by Allen (1963).

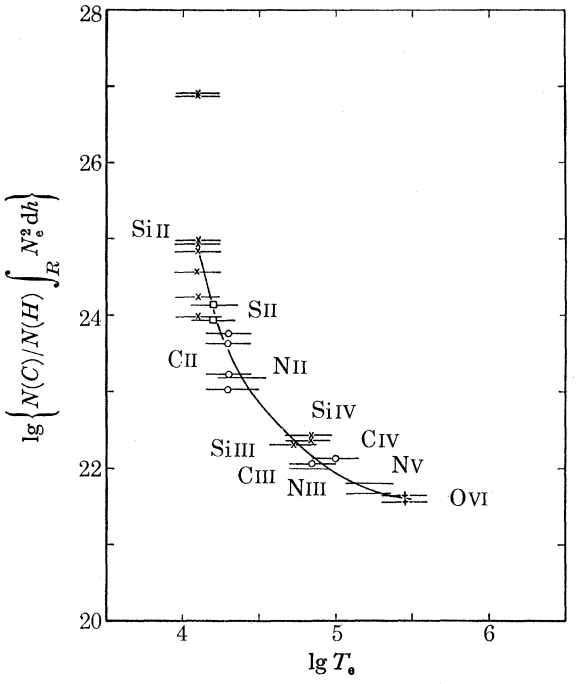

FIGURE 1. Lg $\left\{N(C)/N(H) \int_R N_e^2 \mathrm{d}h\right\}$ as a function of temperature.

TABLE 2. ATOMIC DATA FOR ANALYSIS OF ABSOLUTE DISK INTENSITIES, AND RESULTING VALUES OF $\dfrac{N(E)}{N(H)} \int_R N_e^2 \mathrm{d}h$

ion	λ/nm	lg f	lg $\bar{g}$	lg T_e	$\lg \dfrac{N(E)}{N(H)} \int_R N_e^2 \mathrm{d}h$
C II	103.6	−1.23	−0.27	4.30	23.63
	103.7	−1.23	−0.27	4.30	23.77
	133.4	−0.59	−0.19	4.30	23.02
	133.5	−0.57	−0.19	—	23.23
C III	97.7	−0.09	−0.30	4.85	22.06
C IV	154.8	−0.72	−0.17	4.99	22.13
	155.0	−1.02	−0.17	—	22.13
N II	108.5	−0.85	−0.19	4.40	22.47
N III	98.8	−0.75	−0.19	4.87	21.30
	98.9	−0.75	−0.19	—	21.37
N V	123.8	−0.81	−0.11	5.22	20.96
	124.2	−1.11	−0.11	—	21.10
O VI	103.1	−0.88	−0.07	5.46	21.86
	103.7	−1.19	−0.07	—	21.94
Si II	119.0	−0.48	−0.51	4.10	23.85
	126.0	−0.30	−0.60	4.10	23.37
	126.4	+0.02	−0.60	—	23.52
	130.9	−1.05	−0.48	4.10	24.13
	152.6	−0.96	−0.48	4.10	24.28
	153.3	−0.96	−0.48	—	24.23
	181.7	−1.82	−0.37	4.10	26.18
	180.8	−2.12	−0.37	—	26.20
Si III	120.6	+0.27	−0.39	4.74	21.59
Si IV	139.3	−0.29	−0.32	4.85	21.72
	140.2	−0.59	−0.32	—	21.65
S II	125.3	−1.02	−0.24	4.20	22.94
	125.9	−0.80	−0.24	—	22.72

PHILOSOPHICAL TRANSACTIONS OF THE ROYAL SOCIETY A MATHEMATICAL, PHYSICAL & ENGINEERING SCIENCES

Two features in figure 1 need some comment. The first is the large scatter in the Si II points. This has previously been discussed by Jordan (1969*b*), and is due partly to excitation from the metastable ^4P level which is not included at present, partly to the uncertainty in excitation rates from the ground level, and perhaps also to the sensitivity to temperature of the excitation rates. The second feature is the behaviour of the lines from the Be I-like and Li I-like ions, C III, C IV, and of lines from the Mg I-like and Na I-like ions, Si III, Si IV. It can be seen that C III, and Si III lie below the mean curve, while Si IV and C IV lie above the mean curve.

TABLE 3. ABUNDANCES, TAKING $N(C)/N(H)$ FROM ALLEN (1963) AS STANDARD

element	$\lg(N(E)/N(H))+12$
C	8.50
N	7.80
O	8.80
Si	7.80
S	7.30

The collision strengths used in the present calculations are calculated using the impact-parameter method. This method gives results which for Li I-like ions are close to the more precise calculations of Burke, Tait & Lewis (1965). However, Eissner (private communication) has recently calculated the collision strengths for the resonance lines of the Be I-like ions and his results show that both the impact-parameter method and the results of Osterbrock (1970) overestimate the collision strengths, in C III by a factor of 1.6.

More accurate calculations for other ions are also needed, and the improved collision strengths should reduce the remaining scatter in figure 1.

The scatter in figure 1 is considerably less than that in the previous analyses by Pottasch (1963, 1964) or Athay (1966); apart from the use of more recent atomic data one reason for this may be because the present intensity data refer to a region of the quiet disk and not to integrated emission from the whole Sun.

(*b*) *Derivation of models from the mean* $\int_R N_e^2 \mathrm{d}h$ *distribution*

Following Jordan (1965) (a similar method has been independently derived by Athay (1966)), the integral can be re-written as

$$\int_R N_e^2 \mathrm{d}h = \int_{\lg T_1}^{\lg T_2} N_e^2 \frac{\mathrm{d}h}{\mathrm{d}\lg T_e} \mathrm{d}\lg T_e,$$

where $\lg T_1$ and $\lg T_2$ are $\lg T_m \pm 0.15$ dex.

Assuming (i) $\mathrm{d}h/\mathrm{d}\lg T_e$ is constant over $\Delta T = T_2 - T_1$, and (ii) P_e is constant over ΔT,

$$\int_R N_e^2 \mathrm{d}h = \frac{[P_e^2]_{\Delta T}}{T_m^2} \left[\frac{\mathrm{d}h}{\mathrm{d}\lg T_e}\right]_{\Delta T} \times 0.30, \tag{5}$$

where $P_e = N_e T_e$, and is proportional to the electron pressure.

Both the inner corona and low chromosphere are in hydrostatic equilibrium. Considering a mean model, and ignoring features such as spicules, it will be assumed that the transition region is also in hydrostatic equilibrium. Then,

$$\frac{\mathrm{d}\lg P_e}{\mathrm{d}\lg T_e} = -1.7 \times 10^{-4} \frac{1}{T_e} \frac{\mathrm{d}h}{\mathrm{d}\lg T_e}. \tag{6}$$

Starting from a known pressure at a known height, the pressure gradient and the temperature

gradient can be found from equations (5) and (6). The range of possible pressures is given by the coronal value of 3×10^{14} ($T_e = 1.5 \times 10^6$ K; $N_e = 2 \times 10^8$ cm^{-3}) and the chromosphere value of

$$1.3 \times 10^{15} \quad (T_e = 8 \times 10^3 \text{ K}; N_e = 1.6 \times 10^{11} \text{ cm}^{-3}).$$

Three models (i) with $N_e T_e = 3 \times 10^{14}$ at $T_e = 3 \times 10^5$ K, (ii) with $N_e T_e = 5.6 \times 10^{14}$ at $T_e = 3 \times 10^5$ K and (iii) $N_e T_e = 1.2 \times 10^{15}$ at $T_e = 3 \times 10^5$ K, are shown in figure 2. The starting height is arbitrary and only relative heights are derived. Using data for the range of temperatures 10^4 K to 2×10^6 K, and considering boundary conditions set by eclipse observations, Jordan (1965) found that the best pressure to use is $N_e T_e = 5.6 \times 10^{14}$ at $T_e = 3 \times 10^5$ K. The model derived with this pressure is given in table 4.

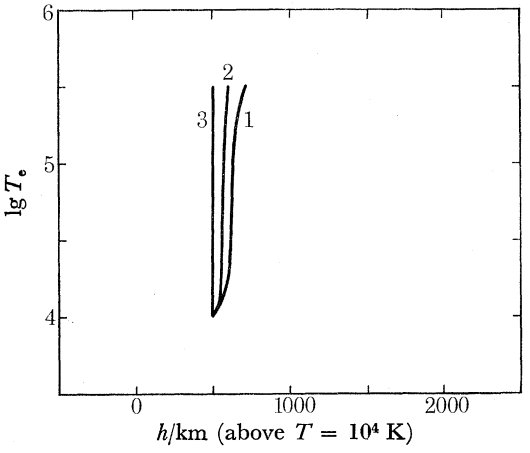

FIGURE 2. Models derived from the absolute disk fluxes. $N_e T_e$ at lg $T_e = 5.5$: model 1, 14.50; model 2, 14.75; model 3, 15.11.

TABLE 4. MODEL DERIVED FROM ABSOLUTE DISK FLUXES

h/km (above $T = 10^4$ K)	lg N_e	lg T_e	$\frac{dh}{d \lg T}$ km/dex
50	10.71	4.1	502
59	10.57	4.2	87
63	10.46	4.3	41
65	10.36	4.4	25
67	10.26	4.5	20
69	10.15	4.6	15
70	10.05	4.7	15
72	9.95	4.8	15
74	9.85	4.9	16
75	9.75	5.0	19
78	9.65	5.1	22
80	9.55	5.2	28
84	9.45	5.3	38
90	9.35	5.4	55
98	9.25	5.5	85

(*c*) *Optical depths*

This model may now be used to calculate the optical depths which are needed in the analysis of the limb to disk ratios. The optical depth can be expressed in terms of the absorption coefficient at the line centre, in the form

$$\tau_h = 1.2 \times 10^{-15} \lambda_{12} f_{12} M^{\frac{1}{2}} \frac{N(E)}{N(H)} \int_{\Delta h} \frac{N(\text{ion})}{N(E)} N_H T_e^{-\frac{1}{2}} dh, \qquad (7)$$

where τ_h is the optical depth at the centre of the disk, and M is the atomic mass of the atom. For $T_e > 2 \times 10^4$ K, $N_H = 0.80 N_e$ as before. The quantity inside the integral is similar to that in the expression for the absolute intensities. The computed values of τ depend therefore on the absolute intensities from which

$$\int_R N_e^2 \, dh$$

is derived, and on the value of $N_e T_e$ used. This point will be discussed again in § 6 (*c*) in connexion with the analysis of limb to disk ratios of 'intermediate' lines.

5. Analysis of limb/disk ratios

It is assumed that the atmosphere is spherically symmetrical, but departures from this do not affect the results of the analysis of optically thin lines if the size of the inhomogeneities is less than the width of the combined slit function. Analysis of optically thick lines can reveal any inhomogeneities. The final equations used for the analysis are given below; a more complete derivation is given in appendix I.

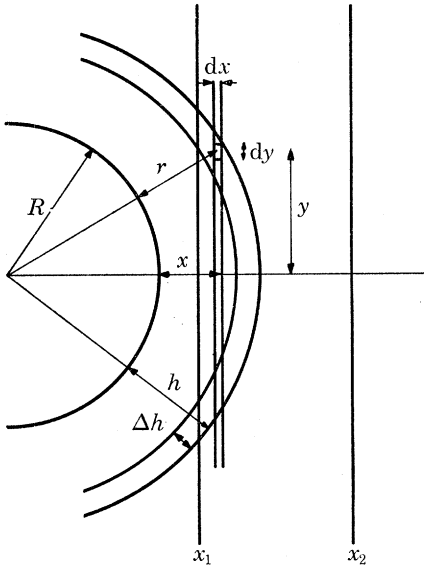

Figure 3. The geometry of an emitting layer and spectrograph slit at the solar limb.

(*a*) *Lines which are optically thin on the disk and at the limb*

The precise equation for the ratio of intensities at the centre of the disk and at the solar limb is

$$\frac{I(\text{limb})}{I(\text{disk})} = \frac{2\pi \int_{-\infty}^{+\infty} \int_{x}^{\infty} f(x - x_0)\, \epsilon(r)\, dr\, dx}{\Delta x \int_0^{\infty} \epsilon(r)\, dr}, \tag{8}$$

where the disk intensity is reduced to a projected slit length R, $\epsilon(r)$ is the volume emission function, Δx is the slit width, $f(x - x_0)$ is the combined image and slit function, dr is an element of length in the radial direction, x is the projected height above the limb, dx is an element of the projected height, and x_0 is the peak of the slit function (see figure 3).

Restricting the emission to a step function, such that

$$\int_x^\infty \epsilon(r)\,\mathrm{d}r = \epsilon_h \Delta h \quad \text{for} \quad h > x$$
$$= 0 \quad \text{for} \quad h < x,$$

where Δh is the thickness of the layer, equation (8) becomes

$$\frac{I(\text{limb})}{I(\text{disk})} = \frac{2\pi}{\Delta x}\int_{-\infty}^{h} f(x-x_0)\,\mathrm{d}x, \tag{9}$$

which is independent of the emission function and depends only on the combined slit function $f(x-x_0)$.

(b) Lines which are optically thick on the disk and at the limb

If the optical depth greatly exceeds unity, then for a layer with constant source function, the relative intensity at the centre of the disk and at the limb is given by the relative areas observed.

The limb/disk ratio is then given by

$$\frac{I(\text{limb})}{I(\text{disk})} = \frac{2}{\Delta x}\left(\frac{2}{R}\right)^{\frac{1}{2}}\int_{-\infty}^{h} (h-x)^{\frac{1}{2}} f(x-x_0)\,\mathrm{d}x, \tag{10}$$

where R is the solar radius.

The heights derived in this case will be approximately the height at which the layer viewed at the limb becomes optically thin ($\tau \sim 1$).

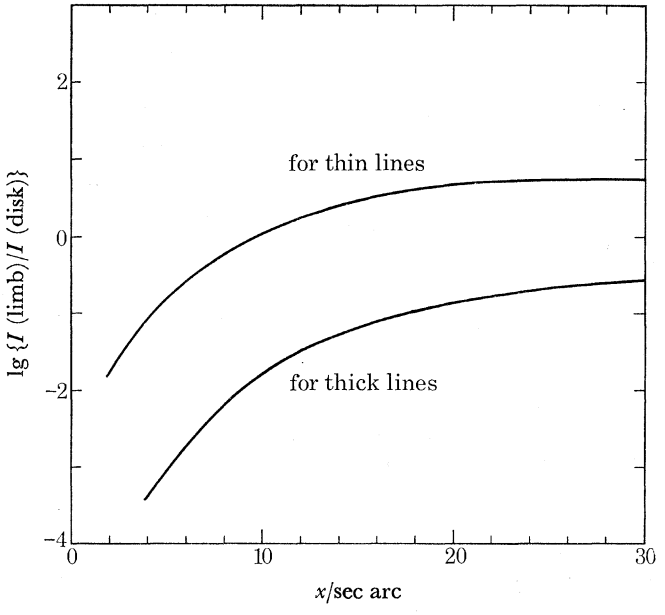

FIGURE 4. The functions $\int_0^x f(x-x_0)\,\mathrm{d}x$ and $\int_0^x (h-x)^{\frac{1}{2}} f(x-x_0)\,\mathrm{d}x$.

(c) Lines which are optically thin on the disk but thick at the limb

Suppose a line is thin on the disk, but has optical depth greater than unity for the regions observed at the limb. One way of treating the limb emission is to consider that it originates from the region in the line of sight up to the point where the optical depth, τ, is unity. This length will be defined as $L(\tau = 1)$.

The limb/disk ratio is then

$$\frac{I(\text{limb})}{I(\text{disk})} = 2\left(\frac{2}{R}\right)^{\frac{1}{2}} \frac{1}{\Delta x} \frac{L(\tau = 1)}{\Delta h} \int_{-\infty}^{h} (h-x)^{\frac{1}{2}} f(x-x_0)\, \mathrm{d}x$$

or, in terms of τ_h, the optical depth of the layer at the centre of the disk, using

$$\frac{L(\tau = 1)}{1} = \frac{\Delta h}{\tau_h},$$

$$\frac{I(\text{limb})}{I(\text{disk})} = \frac{2}{\Delta x}\left(\frac{2}{R}\right)^{\frac{1}{2}} \frac{1}{\tau_h} \int_{-\infty}^{h} (h-x)^{\frac{1}{2}} f(x-x_0)\, \mathrm{d}x. \tag{11}$$

Hence the height of the emitting region cannot be found unless the optical depth at the centre of the disk is also known.

The integrated slit functions used in the analysis are illustrated in figure 4.

6. The structure from limb/disk ratios

Table 5 gives the wavelengths, stage of ionization, temperature of region of formation, optical depths at the centre of the disk, and the height derived for each line. The lines in table 5 are divided into three categories according to their optical depths. Group (*a*) contains those lines which are certainly optically thin both at the centre of the disk and at the limb. These are intercombination lines, lines between excited levels of He II, and resonance lines of N III, N V and Fe II. Group (*b*) contains those lines which have optical depth greater than 50 at the centre of the disk. The third group (*c*) contains the remaining lines. The optical depths have been calculated from the model derived in § 4, using equation (7). For $T < 10^4$ K the model used is based on that of Thomas & Athay (1961). The curve of $\int N_e^2 \mathrm{d}h$ from the extreme u.v. observations is uncertain below $T = 3 \times 10^4$ K since the temperatures at which the lines of singly charged ions are formed are uncertain. The computed optical depths for $T \lesssim 3 \times 10^4$ K are therefore reliable only to within an order of magnitude.

(*a*) *The structure from optically thin lines*

The height, on a relative scale, of formation of each line has been found from equation (9), using the slit function illustrated in figure 4. The height from each line is the average height of emission for that line. Inhomogeneities will not affect the relative heights of lines formed in different temperature regions if the height of the inhomogeneities is less than the width of the slit function, in this case about 30″ or 21 700 km. The results are shown in figure 5. It is apparent that these are consistent with a steep rise in temperature between 1.2×10^4 K and 2.2×10^5 K. The heights derived from Fe II are those found using the accepted coronal abundance of 4×10^{-5}. These lines would, of course, remain optically thin using a lower abundance. Only lower limits are available for the lines of C III and Si III since these lines are too weak to be observed in the disk spectra. The uncertainty in the height for each line, at $h \approx 6500$ km (on the relative scale), assuming that the limb/disk ratios are correct to within a factor of two, is ± 700 km. For $h > 5000$ km the uncertainty in the integrated slit function is less than 700 km. In principle it is possible to determine the relative intensities to $\pm 25\,\%$, and it is hoped that this will be achieved in the next flight. The uncertainty in the height of a transition region ion would then be only ± 350 km.

(*b*) *The structure from optically thick lines*

For a uniform atmosphere, the height derived from the limb/disk ratio of a line which is optically thick at the centre of the disk and at the limb would be the height of the top of the emitting layer. The lines listed in group (*b*) of table 5 all have computed optical depths greater than 50, at the centre of the disk. The heights derived using equation (10) are shown in figure 5.

It is apparent from table 5 (and figure 5) that the heights derived for optically thick lines are

TABLE 5. HEIGHTS DERIVED FROM LIMB/DISK RATIOS AND THE OPTICAL DEPTHS OF LINES USED IN THE ANALYSIS

λ/nm	ion	lg(T_e/K)	lgτ_h	h/sec arc
	(*a*) optically thin lines			
145.5	Ni II	4.1	<-2	4.1
156.7	Fe II	4.1	-2.11	7.7
161.1	Fe II	4.1	-3.48	8.8
161.3	Fe II	4.1	-2.30	8.1
162.3	Fe II	4.1	-3.35	8.2
162.5	Fe II	4.1	-2.42	9.1
163.3	Fe II	4.1	-3.48	7.4
164.9	Fe II	4.1	-2.04	8.1
165.4	Fe II	4.1	-2.27	9.9
167.4	Fe II	4.1	-2.55	9.3
168.6	Fe II	4.1	-2.15	8.4
189.2	Si III	4.70	<-7	>5.6
190.9	C III	4.85	<-7	>6.9
99.1	N III	4.87	-2.21	8.3
108.5	He II	4.9	$\ll 0$	7.4
164.0	He II	4.9	$\ll 0$	9.2
148.7	N IV	5.11	<-5	10.5
140.1	O IV	5.15	<-5	10.0
123.9	N V	5.22	-2.90	9.2
124.3	N V	5.22	-3.20	9.3
121.8	O V	5.35	<-6	8.8
	(*b*) optically thick lines			
157.1	Si I	3.8	~ 3	$>\int$
159.2	Si I	3.8	~ 3	$>\int$
159.8	Si I	3.8	~ 3	$>\int$
132.3	S I	3.8	~ 3	22.2
142.5	S I	3.8	~ 3	15.8
143.3	S I	3.8	~ 3	14.1
147.4	S I	3.8	~ 3	18.2
148.3	S I	3.8	~ 3	18.8
154.5	C I	3.9	~ 2.2	16.6
136.4	C I	3.95	~ 2.8	16.9
126.6	C I	4.0	~ 3	29
127.5	C I	4.0	~ 3	20
146.7	C I	4.0	~ 3	13.8
156.1	C I	4.0	~ 3	22.8
165.7	C I	4.0	~ 3	16.8
130.2	O I	4.0	~ 3	21.8
130.4	O I	4.0	~ 3	18.8
130.6	O I	4.0	~ 3	20.1
119.0	Si II	4.1	~ 3	$>\int$
126.0	Si II	4.1	~ 3	$>\int$
126.5	Si II	4.1	~ 3	$>\int$
130.9	Si II	4.1	~ 2	21.7
152.7	Si II	4.1	~ 2	24.0
153.3	Si II	4.1	~ 2	$>\int$
94.9	H I	4.20	1.78	16.4
102.5	H I	4.20	2.58	18.8
	(*c*) intermediate lines			
147.3	S I	3.8	-1.55	9.0
135.8	O I	3.8	-1.64	9.9
155.9	Fe II	4.1	-0.52	21.0
156.4	Fe II	4.1	-0.66	18.8
156.8	Fe II	4.1	-1.58	10.7
157.0	Fe II	4.1	-0.93	16.2
157.4	Fe II	4.1	-1.44	10.4
157.5	Fe II	4.1	-0.98	13.1
158.5	Fe II	4.1	-1.18	12.0
158.8	Fe II	4.1	-1.31	10.0
160.8	Fe II	4.1	$+0.07$	$>\int$
161.8	Fe II	4.1	-0.47	18.9
162.2	Fe II	4.1	-0.23	$>\int$
163.4	Fe II	4.1	-0.49	29
163.7	Fe II	4.1	-1.70	9.4
164.4	Fe II	4.1	-1.86	8.4
166.0	Fe II	4.1	-0.76	17.5
166.3	Fe II	4.1	-1.57	11.4
167.3	Fe II	4.1	-0.96	17.2
167.9	Fe II	4.1	-1.09	14.3
169.7	Fe II	4.1	-1.52	8.4
170.2	Fe II	4.1	-0.35	22.6
171.3	Fe II	4.1	-0.48	21.2
172.6	Fe II	4.1	-0.96	15.3
180.8	Si II	4.1	$+1.2$	<17.0
181.7	Si II	4.1	$+1.2$	<12.4
125.4	S II	4.20	-0.66	14.8
125.9	S II	4.20	-0.43	20.5
103.6	C II	4.30	-0.62	14.2
103.7	C II	4.30	-0.32	18.7
133.4	C II	4.30	$+0.37$	26
133.6	C II	4.30	0.0	20
108.6	N II	4.40	-1.05	11.4
120.6	Si III	4.70	-1.74	>6.6
130.1	Si III	4.70	-1.75	<7.5
97.7	C III	4.85	-1.20	7.9
117.6	C III	4.85	-1.67	7.8
139.4	Si IV	4.85	-1.96	6.7
140.3	Si IV	4.85	-2.26	6.9
154.8	C IV	5.00	-1.86	6.7
155.1	C IV	5.00	-2.16	6.4
103.1	O VI	5.46	-2.00	7.4
103.8	O VI	5.46	-2.30	7.9

PHILOSOPHICAL TRANSACTIONS OF THE ROYAL SOCIETY A MATHEMATICAL, PHYSICAL & ENGINEERING SCIENCES

considerably larger than those derived from the optically thin lines. There are several possible explanations of these large heights. The optical depth in a line of a neutral atom is certainly very large if the integration is taken down to the temperature minimum between the photosphere

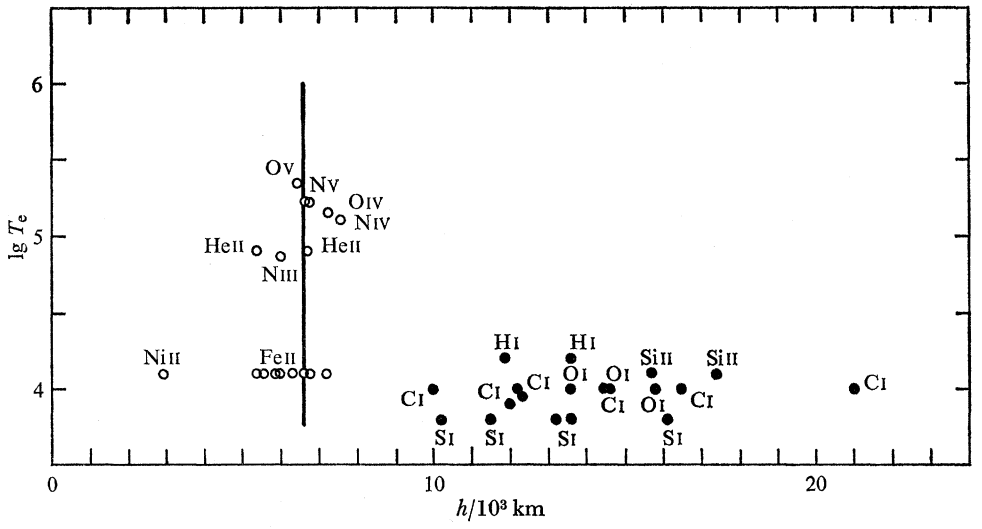

FIGURE 5. The temperature structure derived from (○) lines with $\tau_h < 1$, $\tau_L < 1$; and from (●) lines with $\tau_h > 1$, $\tau_L > 1$.

and chromosphere. It is difficult, however, to find the optical depth over the region from which the observed emission originates without complex calculations of the source function. There is therefore the possibility that some of the tabulated optical depths (except those for lines of neutral hydrogen) are overestimated by an order of magnitude.

But it is possible that the derived heights are realistic. Consider the effect of spicules. If $\tau \sim 50$, the distance to $\tau = 1$ is very small, about 1 km for the hydrogen lines. This is less than the diameter of one spicule, so that spicules superimposed in the line of sight would raise the average height of the top of the emitting layer. Lines of neutral ions would then apparently be formed above lines of the transition region ions in which the spicules are optically thin.

From table 5 it can be seen that if equation (9) is used for the lines of Si I and Si II, no solution for the height can be found, since in the optically thick approximation the limb emission apparently exceeds that given by the total area of the slit function. This effect is almost certainly due to the emission originating in a non-uniform layer. In fact, the lines of neutral atoms originate in a region where there is a steep positive temperature gradient. The limb emission could therefore originate predominantly in a region where the optical depth is smaller and the temperature is greater than in the region where the disk emission originates. For such an effect to be important, these lines must be optically thin in the spicules. The computed optical depths for the Si I and Si II lines are certainly smaller than those of the C I and O I lines.

(*c*) *Intermediate lines*

The lines tabulated in group (*c*) of table 5 are those for which the disk optical depth is less than about 10, but for which the optical depth at the limb could be large due to the long line of sight path length. For a uniform layer, the height can be calculated from equation (11) using the computed optical depths. The derived heights are shown in figure 6, and an overall similarity with figure 5 is apparent.

For the lines of C IV, Si IV and O VI the computed optical depths are fairly insensitive to the model used since the integration for the optical depth and the emission is the same except for a density term and the exponential temperature term. The limb optical depths for these lines are small enough for the spicules to be optically thin to their radiation, and for the uniform layer approximation to be valid.

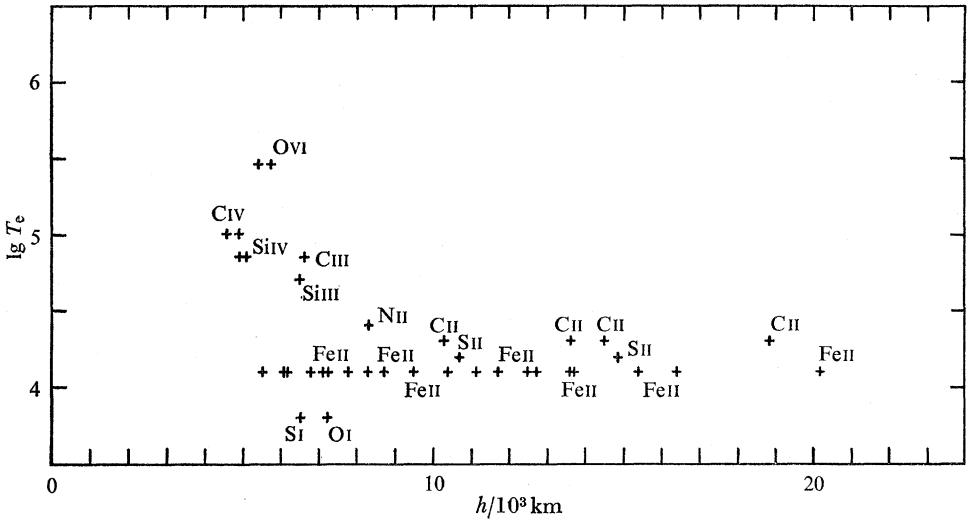

FIGURE 6. The temperature structure derived from lines with $\tau_h < 1$, $\tau_L > 1$.

In order to compute the optical depths in the lines of C III and Si III the population of the metastable ^{3}P level must be known. In figure 6 the resonance lines are plotted assuming that all the population of each ion is in the ground state. The recent calculations of Jordan (1970) can be used to replace this approximation, and more accurate heights for the emission of the resonance line at 97.7 nm and $2s\,2p\,^3P$–$2p^2\,^3P$ lines at 117.5 nm are listed in table 5. For Si III the precise population of the ^{3}P level is not known. Using the Boltzmann population gives a lower limit to the height of the resonance line and an upper limit to the height of the $3s\,3p\,^3P$–$3p^2\,^3P$ line.

The systematically lower heights derived for the intermediate lines (comparing figures 5 and 6) would be removed by a factor of 3 increase in the computed optical depths. This factor of 3 could lie in either the absolute intensities or the electron pressure used in the derivation of the model. In view of the possible error of about a factor of two in the absolute photometry this can be considered reasonable agreement. The absolute intensities from the present flight are systematically lower than those of Tousey *et al.* (1965) by a factor of about 3. Improved photometry would lead to a better check on the electron pressure used in the absolute intensity model.

The discussion (in the previous section) on the possible reasons for the large heights derived for low ions is equally valid for the lines of second ions shown in Figure 6. However, there is a sufficient number of iron lines observed to examine the dependence of the limb/disk ratios on oscillator strength. If lines formed at the same temperature are optically thin their limb/disk ratios should be independent of their optical depths. Within the probable error in the limb/disk ratios this is true of the lines listed in group (*a*) of table 5. If the optical depth at the limb becomes greater than unity the limb/disk ratio should fall below its optically thin value. For a uniform atmosphere the gradient $\Delta \lg (I\,(\text{limb})/I\,(\text{disk}))/\Delta \lg \tau$ should be -1. If the spicules are optically thick to the iron lines or the layer is not uniform in temperature the gradient should be negative

but less steep. The observed limb/disk ratios for the Fe II lines do depart from a constant value for $-2 < \lg \tau_h < -1$, but with a gradient that is less steep than -1. The scatter in the limb/disk ratios is too large in the present data to make definite conclusions about the iron abundance, but there is evidence that an abundance larger than the 'photospheric' value is indicated by the value of τ at which the limb/disk ratios depart from being constant. The oscillator strengths used have been calculated by the method of Bates & Damgaard (1949), and on average may be overestimates of the true values. If this were so an even larger abundance would be required to fit the observed limb/disk ratio variation. On the other hand, increasing τ to allow for an error in the absolute photometry would lead to a smaller abundance being more appropriate. Improved photometry could lead to a determination of the iron abundance from the limb/disk ratios. The lines of S I and O I are intercombination lines which are almost optically thin, and their heights suggest a steep temperature gradient even between 8000 K and 1.3×10^4 K.

7. Conclusions

The temperature structure derived from the limb/disk ratios of optically thin lines is consistent with a steep gradient between 10^4 and 3×10^5 K within the probable error of the photometry.

Although it is difficult to distinguish directly between several models computed from the absolute intensities by comparing with the structure derived from the limb/disk ratios, the lines which are optically thick at the limb provide a check on the electron pressure used in the model. There is evidence from the lines of neutral hydrogen that cool material ($\sim 10^4$ K) extends up to 8000 km into the corona above the transition region, presumably in the form of spicules. Improved photometry could lead to a more accurate determination of the temperature structure and of the electron pressure, and to a determination of the abundance of iron in the chromosphere.

Revision

This paper is a revised version of that given at the Royal Society Meeting on Solar Studies in April 1970. The revisions are due to improvements in the intensity calibration used. The revision of the calibration did not affect the analysis of the limb to disk intensity ratio, but reduced the scatter in the absolute intensity data. In particular, the large anomaly in the relative intensities of lines from Be I-like and Li I-like ions has been reduced to the point where improved collision strengths should account for the remaining difference.

Appendix I. Derivation of equations for limb/disk analysis

(*a*) *For lines which are optically thin on the disk and at the limb*

Consider an element of atmosphere of width dx at projected height x above the limb, and radial distance r from the limb (see figure 3). Let this element be part of a ring of thickness dy and radius y. The emission from this ring is given by

$$2\pi\epsilon(r)\, y\, \mathrm{d}y\, \mathrm{d}x,$$

where $\epsilon(r)$ is the volume emission coefficient.

The emission from the plane parallel slab of thickness dx is then

$$\mathrm{d}E = 2\pi\, \mathrm{d}x \int_0^\infty \epsilon(r)\, y\, \mathrm{d}y$$

PHILOSOPHICAL TRANSACTIONS OF THE ROYAL SOCIETY A MATHEMATICAL, PHYSICAL & ENGINEERING SCIENCES

or, using
$$y^2 = (R+r)^2 - (R+x)^2$$
$$2y\,dy = 2(R+r)\,dr,$$

the emission is
$$dE = 2\pi\,dx \int_x^\infty \epsilon(r)\,(R+r)\,dr$$
$$\simeq 2\pi R\,dx \int_y^\infty \epsilon(r)\,dr \quad \text{for} \quad r \ll R.$$

The total flux through a slit of width Δx with jaws at x_1 and x_2 is given by
$$E\,(\text{limb}) = 2\pi R \int_{x_1}^{x_2} \int_x^\infty \epsilon(r)\,dr\,dx. \tag{i}$$

As each emission line is formed close to the temperature at which the ion has its maximum abundance, the integral over dr can be replaced by a step function such that
$$\int_x^\infty \epsilon(r)\,dr = \epsilon_h \Delta h \quad \text{for} \quad h > x$$
$$= 0 \quad \text{for} \quad h < x$$

where Δh is the effective width of the layer.

Then
$$I\,(\text{limb}) = 2\pi R \epsilon_h \Delta h \int_{x_1}^h dx$$
$$= 2\pi R \epsilon_h \Delta h (h - x_1),$$

where h is the radial height of the top of the layer above the limb.

In practice, owing to aberrations and pointing errors, the slit function projected at the source is not rectangular but is smeared out into some function $f(x-x_0)$, where x_0 is the peak of the distribution but is essentially an arbitrary constant. The function is normalized so that
$$\int_{-\infty}^{+\infty} f(x-x_0) = \Delta x.$$

Equation (i) now becomes
$$I\,(\text{limb}) = 2\pi R \int_{-\infty}^{+\infty} f(x-x_0) \int_x^\infty \epsilon(r)\,dr\,dx, \tag{ii}$$

or restricting the emission to Δh as before
$$I\,(\text{limb}) = 2\pi R \epsilon_h \Delta h \int_{-\infty}^h f(x-x_0)\,dx. \tag{iii}$$

The disk flux, from an area covered by a slit of width Δx and length R is
$$I\,(\text{disk}) = R\,\Delta x \int_0^\infty \epsilon(r)\,dr$$
$$\simeq R \Delta x \epsilon_h \Delta h.$$

From equations (ii) and (iii), the limb/disk ratio is
$$\frac{I\,(\text{limb})}{I\,(\text{disk})} = \frac{2\pi}{\Delta x} \int_{-\infty}^h f(x-x_0)\,dx.$$

(b) For lines which are optically thick on the disk and the limb

If the optical depth exceeds unity then for a layer with constant source function the relative intensity at the centre of the disk and at the limb is given by the relative areas observed.

The area at the limb is the area of the segment of a circle of radius $(R+h)$ cut by a chord at distance $(R+x_1)$ from the centre. If θ is the angle between the equator and the intersection of the chord and the circle,

$$I(\text{limb}) \propto 2 \times \tfrac{1}{2}(R+h)^2[\theta^c - \sin\theta\cos\theta].$$

In practice θ is small. Hence

$$I(\text{limb}) \propto \tfrac{4}{3}[2R]^{\frac{1}{2}}(h-x_1)^{\frac{3}{2}}.$$

Replacing the slit by a slit function as before,

$$I(\text{limb}) = 2(2R)^{\frac{1}{2}}\int_{-\infty}^{h}(h-x)^{\frac{1}{2}}f(x-x_0)\,\mathrm{d}x.$$

The area of the slit on the disk is $R\Delta x$. Hence

$$\frac{I(\text{limb})}{I(\text{disk})} = 2\left(\frac{2}{R}\right)^{\frac{1}{2}}\frac{1}{\Delta x}\int_{-\infty}^{h}(h-x)^{\frac{1}{2}}f(x-x_0)\,\mathrm{d}x. \qquad \text{(iv)}$$

(c) Lines which are optically thin on the disk but thick on the limb

Consider the situation in a plane parallel layer of radial thickness Δh and tangential length L, such that $L \gg \Delta h$, and suppose this layer represents the solar atmosphere viewed at the limb. Let the optical depth at the line centre in the radial direction be τ_h, and let the optical depth in the tangential direction be τ_L. For resonance lines which have $\tau_h \lesssim 10^2$ there will be no destruction of photons by collisional de-excitation, only resonance line scattering. If a photon is re-absorbed the probability for its escape after each scattering will be much greater in the radial direction than in the tangential direction (Holstein 1947). For the simple case considered above and for a Doppler-broadened line the probability of escape is given by

$$q = 1 - \operatorname{erf}(\ln\tau)^{\frac{1}{2}}.$$

The fraction of photons created that escape in the radial direction will be

$$W_h = bq_h/[1-b(1-q_h)],$$

where b is the probability that a photon is emitted in the line under consideration. If $b = 1$ (i.e. assuming there is only one line from the excited level), then

$$W_h = 1.$$

Hence in the radial direction it can be assumed that all photons created in the layer escape.

The fraction of photons created that escape in the tangential direction will be, with $b = 1$,

$$W_L = q_L/[1-(1-q_h)] = q_L/q_h \qquad \text{(v)}$$

as the re-absorption is still determined by the optical depth in the radial direction. The expressions for W_h and W_L are only approximate, which accounts for the apparent contradiction when considering the total emission in all directions. For $\tau_h < 1$ and $\tau_L \gg 1$, $q_h = 1$ and $q_L \to 1/\tau_L$. The limb/disk ratio now becomes

$$[I(\text{limb})/I(\text{disk})]_{\text{Int}} = [I(\text{limb})/I(\text{disk})]_{\text{thin}} \times 1/\tau_L. \qquad \text{(vi)}$$

PHILOSOPHICAL TRANSACTIONS OF THE ROYAL SOCIETY A MATHEMATICAL, PHYSICAL & ENGINEERING SCIENCES

Since the emission included in the limb observations does not come from a simple plane parallel slab, and features such as spicules may be important, the alternative approach of considering that the emission at the limb comes from the depth at which $\tau_L = 1$ is more general.

Define this line of sight distance as $L(\tau = 1)$.

The limb emission, restricting the region of emission in the radial direction to a layer of width Δh as before, and using the slit function $f(x)$, is

$$I(\text{limb}) = 2(2R)^{\frac{1}{2}} \epsilon_h L(\tau = 1) \int_{-\infty}^{h} (h-x)^{\frac{1}{2}} f(x-x_0)\, \mathrm{d}x. \tag{vii}$$

The disk emission is given by equation (iii).

Hence

$$\frac{I(\text{limb})}{I(\text{disk})} = 2\left(\frac{2}{R}\right)^{\frac{1}{2}} \frac{1}{\Delta x} \frac{L(\tau = 1)}{\Delta h} \int_{-\infty}^{h} (h-x)^{\frac{1}{2}} f(x-x_0)\, \mathrm{d}x.$$

By definition,

$$L(\tau = 1)/1 = \Delta h/\tau_h,$$

where τ_h is the optical depth of the layer at the centre of the disk. Then,

$$\frac{I(\text{limb})}{I(\text{disk})} = 2\left(\frac{2}{R}\right)^{\frac{1}{2}} \frac{1}{\Delta x} \frac{1}{\tau_h} \int_{-\infty}^{h} (h-x)^{\frac{1}{2}} f(x-x_0)\, \mathrm{d}x$$

$$= [I(\text{limb})/I(\text{disk})]_{\text{thick}} \times 1/\tau_h. \tag{viii}$$

With $f(x) = 1$ this reduces to

$$[I(\text{limb})/I(\text{disk})]_{\text{int}} = [I(\text{limb})/I(\text{disk})]_{\text{thin}} \times 1/\tau_L.$$

References (Burton *et al.*)

Allen, C. W. 1963 *Astrophysical quantities* (2nd ed.). Athlone Press.

Athay, R. G. 1966 *Astrophys. J.* **145**, 784.

Bates, D. R. & Damgaard, A. 1949 *Phil. Trans. Roy. Soc. Lond.* A **242**, 101.

Black, W. S. & Shenton, D. B. 1966 *The peaceful uses of automation in outer space*. New York: Plenum Press.

Burgess, A. 1964 AERE-R-4818. Harwell: U.K.A.E.A.

Burke, P. G., Tait, J. H. & Lewis, B. A. 1966 *Proc. Phys. Soc.* **87**, 209.

Burton, W. M., Ridgeley, A. & Wilson, R. 1967 *Mon. Not. R. astr. Soc.* **135**, 207.

Burton, W. M., Ridgeley, A. & Hatter, A. T. 1968 Esro Report SP/33. Paris: Esro.

Burton, W. M. & Ridgeley, A. 1970 *Solar Phys.* **14**, 3.

Delache, P. 1967 *Annls Astrophys.* **30**, 827.

Hall, C. A., Damon, K. R. & Hinteregger, H. E. 1963 *Space Res.* **3**, 745.

House, L. L. 1964 *Astrophys. J.* (Suppl.) 81, **8**, 307.

Jordan, C. 1965 Ph.D. Thesis, London University.

Jordan, C. 1969*a* *Mon. Not. R. astr. Soc.* **142**, 501.

Jordan, C. 1969*b* *Astrophys. J.* **156**, 49.

Jordan, C. 1970 To be published in *Highlights of astronomy, 1970*, ed. C. de Jager. Dordrecht, Holland: D. Reidel.

Junkes, J., Salpeter, E. W. & Milazzo, G. 1965 *Atomic spectra in the vacuum ultraviolet*. Part I. Citta del Vaticano: Specola Vaticana.

Kelly, R. L. 1968 N.R.L. Report 6648. Washington D.C.: N.R.L.

Moore, C. E. 1950 NBS Circular 488. Washington D.C.: U.S. Govt. Printing Office.

Moore, C. E. 1965 NSRDS-NBS-T, Section 1. Washington D.C.: U.S. Govt. Printing Office.

Osterbrock, D. E. 1970 *J. Phys.* B **3**, 149.

Pottasch, S. R. 1963 *Astrophys. J.* **137**, 945.

Pottasch, S. R. 1964 *Space Sci. Rev.* **3**, 816.

Thomas, R. N. & Athay, R. G. 1961 *Physics of the solar chromosphere*, pp. 203, 215 and 217. New York–London: Interscience.

Tousey, R., Austin, W. E., Purcell, J. D. & Widing, K. G. 1965 *Annls Astrophys.* **28**, 755.

Wiese, W. L., Smith, M. W. & Glennon, B. M. 1966 NSRDS–BNS–4. Washington, D.C.: U.S. Govt. Printing Office.

PHILOSOPHICAL TRANSACTIONS OF THE ROYAL SOCIETY A MATHEMATICAL, PHYSICAL & ENGINEERING SCIENCES